THE ASTROPHYSICAL JOURNAL, 495:774–785, 1998 March 10
© 1998. The American Astronomical Society. All rights reserved. Printed in U.S.A.

SPECTRA OF MASER RADIATION FROM A TURBULENT, CIRCUMNUCLEAR ACCRETION DISK

B. K. WALLIN, W. D. WATSON, AND H. W. WYLD
Department of Physics, University of Illinois at Urbana-Champaign, Urbana, IL 61801-3080
Received 1997 May 27; accepted 1997 October 20

ABSTRACT

The spectrum of maser radiation from a thin Keplerian disk viewed edge-on is computed when idealized turbulent velocities are present in the disk. Representative turbulent velocity fields ("realizations") are created by statistical sampling from Kolmogorov-like distributions (suggested by simulations) for the turbulence and combined with the Keplerian velocities of rotation. Parameters are chosen for the numerical computations to facilitate a detailed comparison to refined observational data available for the bulk of the maser emission that occurs near the systemic velocity in the subparsec disk of water masers around a presumed massive black hole at the nucleus of the galaxy NGC 4258. Spectra are obtained that are similar in appearance to the irregular spectra that are observed. Microstructure with Doppler breadths comparable to the expected thermal velocities occur in both the observed and computed spectra, even though the turbulent velocities in the computations are much greater than the thermal velocities. The observed deviations in the maser emission from the Keplerian relationship between Doppler velocity and location indicate that the turbulence is somewhat supersonic. It may still be sub-Alfvénic. A relationship between the radial extent of the masing gas and the magnitude of the turbulent velocities is provided by the range of Doppler velocities at which maser emission is observed. The computed spectra are consistent with (but do not require) the presence of a strong continuum source that is being amplified by the masing disk and that is associated with the presumed black hole at the nucleus of the galaxy.

Subject headings: accretion, accretion disks — Galaxy: center — ISM: kinematics and dynamics — masers — turbulence

1. INTRODUCTION

Spectral line emission indicates that irregular velocities (turbulence or waves) are pervasive in the diffuse gas in astronomical environments on a wide range of spatial scales. Only a few efforts have, however, been made to calculate the appearance of spectral line features formed in a turbulent gas. Because of its "exponential amplification," maser radiation is especially sensitive to irregularities in the masing medium. It is then not surprising that the maser emission in our own Galaxy, which can be spatially resolved, tends to appear as "spots" that often exhibit motions and time variability. The relative importance of variations in the velocity field versus variations in the excitation is, in general, unclear. From another perspective, velocity irregularities in the form of waves and turbulence are intimately involved in considerations about the pressure and viscosity in accretion disks and in regions of star formation. Compelling evidence for such velocities based on the "excess breadths" of spectral lines exists for regions of potential star formation. The focus in this paper is accretion disks and, in particular, the subparsec disk of 22 GHz water masers around the presumed black hole at the nucleus of the galaxy NGC 4258. The cause for the viscosity in all types of astrophysical accretion disks is an outstanding issue. In standard viewpoints, the turbulent velocities may be comparable to the thermal velocities to create sufficient viscosity to satisfy astrophysical constraints (alpha near unity in "alpha-viscosity"). The availability of observational information about the masing disk in NGC 4258 that is both extensive and refined provides motivation for this investigation. The narrow spectral lines (as small as 1 km s^{-1}) and small spot sizes (less than about 10^{13} cm in our own Galaxy), together with their high surface brightnesses, enhance the value of masers as indicators of astronomical phenomena.

Certain simplifying idealizations are adopted here. (1) The masing is calculated in the unsaturated limit. We reason in § 3.1 that this is a justifiable approximation for the maser radiation from NGC 4258 that we are attempting to describe—that near the systemic velocity of that galaxy. (2) The "pumping" for the maser, or more precisely the opacity κ_o, is taken to be constant between the inner and outer radius of a masing ring within a Keplerian disk. The observational evidence that the locations of maser emission from NGC 4258 are determined mainly by the velocity gradients in a Keplerian velocity field indicates that there is some uniformity in κ_o, at least on length scales comparable to the coherence length resulting from the Keplerian velocity gradients. That is, the characteristic "triplet" spectrum of a Keplerian disk with constant opacity is evident in the observations and played a key role in the original identification of the disk (Watson & Wallin 1994). In addition, certain mechanisms that have been recognized as likely for creating the masing environment tend to produce extended rather than concentrated regions (Collison & Watson 1995; Desch, Wallin, & Watson 1998). (3) Finally, representative turbulent velocity fields are created by statistical sampling ("realizations") utilizing Kolmogorov-like distributions for the power spectrum of the velocities and Gaussian distributions for the amplitudes. These methods have long been standard in fluid mechanics (e.g., Lesieur 1990) and have been used, for example, in a somewhat related context by Dubinski, Narayan, & Phillips (1995, hereafter DNP) for creating velocity distributions in regions of star formation. These velocities are viewed by us as turbulent velocities in the rotating frame of the disk so that they can simply be added to the Keplerian velocities of rotation to obtain the velocities of the masing medium in relation to the observer. Clearly this is an idealization. Obtaining a quantitative

description of a turbulent, rotating MHD medium (potentially including heating and cooling mechanisms, chemical reactions, etc.) is a discipline in itself where such issues are only just beginning to be addressed. That our approach is not unreasonable is suggested by the tendency for power-law dependences similar to Kolmogorov to appear in a wide range of calculations for turbulence in various environments. Kolmogorov-like dependencies seem to appear in the calculations for MHD turbulence in Keplerian disks that have been performed (Brandenberg et. al. 1995; Stone et al. 1996). In accretion disks, the turbulent energy is expected to be injected at wavelengths comparable to the thickness of the disk, and is expected to be anisotropic due to the rotation and the geometry. These properties are reflected in the results of the limited numerical simulations. We utilize analytic approximations that reflect these basic properties. Creating velocity fields from the power spectra automatically eliminates "intermittencies," or long-wavelength features that appear in some simulations for turbulence. We expect that most of the energy in the turbulent velocities of an accretion disk is due to instabilities related to the thickness of the disk. Limiting our attention to variations in the turbulent velocities with characteristic wavelengths much less than the radius of a thin disk can thus be justified. Variations at longer wavelengths than we treat may occur, but seem more likely to be due to phenomena such as the creation of spiral arms.

The basic methods and geometry are presented in § 2, where we describe the techniques for creating representative turbulent velocities. Spectral and spatial distributions of the maser flux that are computed to provide a basis for interpreting the disk in NGC 4258 are given in figures in § 3. Close comparisons are made to the observational data. Conclusions that can tentatively be drawn based on these comparisons are summarized in the concluding section, § 4. Understanding whether the spectral features (or clumpiness) that are evident in the observational data can be understood mainly as a consequence of the turbulence and determining the magnitude of the implied turbulent velocities are central issues in the interpretation. The investigation here addresses neither the time variations in the spectra nor the creation of the "high-velocity" spectral features from the sides of the disk. These will be examined in future investigations that build upon the methods and experience acquired here.

2. BASIC METHODS

2.1. *Creating the Velocity Fields*

The turbulent velocity fields described below are viewed as being defined in the frame rotating with the disk. To obtain velocities in the observer's frame, they are superposed onto the much greater velocities of the Keplerian rotation of the disk simply by adding these two velocities. Snapshots in time or statistical realizations of the turbulent velocities are obtained by Fourier expansion utilizing a Gaussian distribution for the amplitudes of the Fourier components and Kolmogorov-like forms for the power spectra as a function of the wavenumbers of the velocities. In particular, we follow the description of DNP where these methods are applied in a context that is somewhat similar to our own. In the Kolmogorov description, the fluid is treated as incompressible. This incompressibility is further exploited in order to derive the turbulent velocity from a vector potential $\boldsymbol{A}$ through $\boldsymbol{v} = \nabla \times \boldsymbol{A}$ (since $\nabla \cdot \boldsymbol{v} = 0$). The Kolmogorov power spectrum for the velocity $P_v(k) \equiv |\boldsymbol{v}_k|^2 \propto k^{-11/3}$ at wavenumber $k = |\boldsymbol{k}|$ leads to the power spectrum $P_A(k) \equiv \langle |\boldsymbol{A}_k|^2 \rangle \propto k^{-17/3}$ for the Fourier components of $\boldsymbol{A}$ that are described by a Gaussian distribution. Gas in astrophysical environments is far from incompressible. Other than simplicity, the partial justification (DNP) is that incompressibility leads to the Kolmogorov form that (as noted in § 1) tends to emerge in a wide range of simulations, including some for accretion disks. To prevent an increase in the spectrum at wavenumbers that are smaller than those at which energy is believed to be injected into the gas of the disk, as well as a divergence at small wavenumbers, a cutoff wavenumber $k_{\rm min}$ is introduced so that $P_A(k) \equiv \langle |\boldsymbol{A}_k|^2 \rangle \propto (k^2 + k_{\rm min}^2)^{-17/6}$. In practice, the real and imaginary parts of each Cartesian component of $\boldsymbol{A}_k$ are chosen separately. For example, for the real part of the y component A_k^{ry},

$$\langle |A_k^{ry}|^2 \rangle = \sigma_A^2 = C(k^2 + k_{\rm min}^2)^{-17/6} . \quad (1)$$

In creating a statistical realization, its amplitude at wavenumber $\boldsymbol{k}$ is then chosen from a Gaussian probability distribution $f(A_k^{ry})$ using a random number generator,

$$f(A_k^{ry}) = [(2\pi)^{1/2}\sigma_A]^{-1} e^{(-A_k{}^{ry})^2/2\sigma_A{}^2} . \quad (2)$$

Exactly the same procedure (with the same constant C) is followed in choosing the imaginary part A_k^{iy} and in choosing the real and imaginary parts of the z component of $\boldsymbol{A}_k$. After obtaining the set of $\boldsymbol{A}_k$, the Fourier transform of the velocity $\boldsymbol{v}_k$ is calculated from

$$\boldsymbol{v}_k = i\boldsymbol{k} \times \boldsymbol{A}_k \quad (3)$$

and the velocity field in real space is computed by taking the inverse Fourier transform of $\boldsymbol{v}_k$.

Only two components of the vector potential are needed, since the calculated fluxes of radiation will depend only upon the component v_t of the turbulent velocity that is along the line of sight and parallel to the x-axis. Fast Fourier transform methods are utilized in a box that is $512 \times 512 \times 32$ grid points for most computations. The appropriateness of this size is discussed in § 3. When summed over all grid points, the distribution of v_t is essentially a Gaussian for each realization and has a mean square velocity σ_t^2. Note that σ_t^2 refers only to the component of the turbulent velocity that is parallel to the line of sight.

Although σ_t^2 depends upon both $k_{\rm min}$ and C, we take $k_{\rm min}$ to be $2\pi/H$ and adjust C accordingly to create the specified value for σ_t^2. It is expected that the turbulent fluctuations will be injected into the medium with wavelengths approximately equal to the thickness H of the disk (e.g., Brandenburg et. al. 1995; Stone et. al. 1996).

The volume in which we wish to create realizations of the velocity field is an extended portion of a disk and is not cubic. The range of Doppler velocities evident in the emission near the systemic velocity of NGC 4258 indicates that the maser radiation is created within a range of impact parameters ($\simeq 4 \times 10^{16}$ cm) on either side of the center that is about 1/10 of the radius at which the masing occurs. Although the thickness of the disk may be smaller (see § 3.1), most of our calculations are based on a thickness H of 5×10^{15} cm. A limited number of computations have been performed with $H = 10^{15}$ cm. No significant differences were evident. The exact radial extent of the region in which

the maser radiation is created is uncertain. It is one of the parameters in our calculations to be determined (or at least restricted) by a comparison to the observational data. We wish to consider the possibility that the radial extent is at least as large as one-fifth of the disk radius, as suggested by certain interpretations of the data. The basic rectangular volume in which statistical realizations of the velocity field are created in our calculations is thus chosen to be $16H \times 16H \times H$ and is positioned as indicated in Figure 1 in relation to the disk. The $512 \times 512 \times 32$ array that is used in our computations then provides equal spacings in the three directions for the locations at which the velocities are computed. These foregoing choices thus lead to a range of wavenumbers associated with each direction i that lies in the range

$$-\frac{1}{2}\left(\frac{2\pi}{L_i}\right)n_i^{\max} \leq k_i \leq +\frac{1}{2}\left(\frac{2\pi}{L_i}\right)n_i^{\max}, \quad (4)$$

where $L_i = 16H$ or H and the integers $n_i^{\max}$ are either 512 or 32, respectively, depending upon whether the direction i is within the plane of or perpendicular to the disk.

Although the power spectrum of equation (1) does limit the contributions in the plane of the disk at wavelengths greater than H as is desirable, it does not reflect an anisotropy at shorter wavelengths as might also be expected and which does appear in numerical simulations. To reflect the approximate factor of 1000 difference in $\langle |\boldsymbol{v}_k|^2 \rangle$ at wavelengths shorter than H when $\boldsymbol{k}$ is parallel to the Keplerian velocity of rotation in comparison to $\langle |\boldsymbol{v}_k|^2 \rangle$ when $\boldsymbol{k}$ is in the other two directions, which is found in the simulations (Brandenberg et al. 1995; Stone et al. 1996), we also utilize the following equation in analogy with equation (1)

$$\langle |A_k^{ry}|^2 \rangle = C[k_x^2 + 11.45k_y^2 + k_z^2 + k_{\min}^2]^{-17/6}, \quad (5)$$

which we designate as the anisotropic spectrum. As for the "isotropic" spectrum of equation (1), the imaginary part A_k^{ry} and the other components of $\boldsymbol{A}_k$ are also obtained from equation (5). In Figure 1, the x and y directions are parallel to the plane of the disk. They are, respectively, parallel and perpendicular to the line of sight. The z direction is perpendicular to the plane.

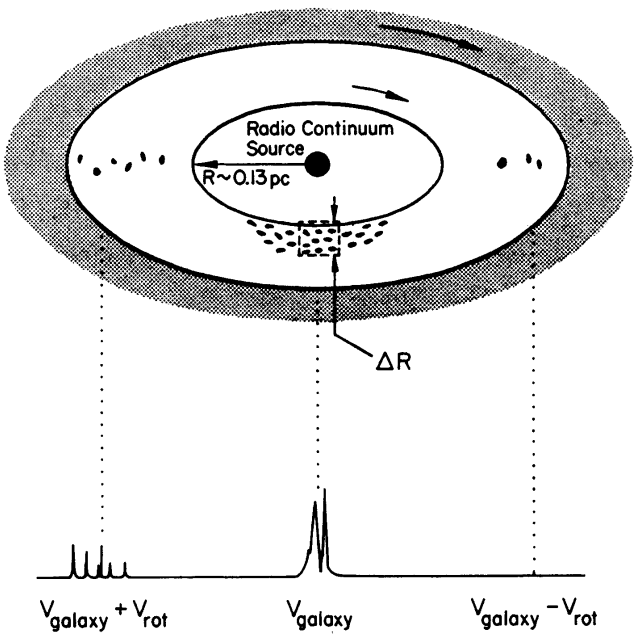


FIG. 1.—Relationship between the volume of turbulent gas (*outlined by dashed lines*) from which the spectra of maser radiation are being computed, and the accretion disk around the presumed black hole at the nucleus of NGC 4258 (not to scale). The rotational velocities are Keplerian and are approximately 1100 km s^{-1} and 800 km s^{-1} at the inner and outer radii of the ring. The radiation from the sides, shifted by plus and minus the rotational velocity, are not considered in this investigation (adopted from Greenhill et al. 1995).

2.2. *Calculating the Observed Spectral Line Radiation*

To calculate the observed flux, note that the distance to the observer is much greater than the dimensions of the disk and that the observer is assumed to view the disk edge-on. Hence, the paths for the rays of the observed radiation are essentially parallel, straight lines within the disk along the x-axis in Figure 1. Since the masing is to be calculated in the unsaturated regime, the optical depth at the frequency that corresponds to the observed Doppler velocity v for a maser ray that is parallel to the plane of the disk and emerges from the disk at an impact parameter b and height z above the midplane is

$$\tau(v, b, z) = \kappa_o \int \exp\left[-(v - v^K - v^t)^2/v_{\rm th}^2\right] ds, \quad (6)$$

where our idealization that the maser opacity κ_o is constant between the inner and outer radii of the masing ring (see § 1) has been utilized. The distance s is measured along the ray. Only the components v^K and v^t of the Keplerian velocity and the turbulent velocity that are parallel to the line of sight enter. The thermal velocity $v_{\rm th} = (2kT/M_{\rm H_2O})^{1/2}$ is taken as $v_{\rm th} = 0.70$ km s^{-1}, which corresponds to $T \simeq 500$ K. The opacity κ_o will be treated as a parameter to be determined by comparison to the observational data since it follows from the pumping rate for the maser, which is uncertain (e.g., Wallin & Watson 1997). For circular motion at radius r around the mass M, the component of the Keplerian velocity along the ray with impact parameter b is

$$v^K = b(GM)^{1/2}/r^{3/2}. \quad (7)$$

Utilizing the above $\tau(v, b, z)$, we can express the intensity of radiation emerging toward the observer from a location (b, z) on the edge of disk as

$$I(v, b, z) = I^C \exp\left[\tau(v, b, z)\right], \quad (8)$$

where I^C is the intensity of the background continuum source at the center about which the disk rotates, or $I^C = 2v^2kT_c/c^2$ in the Rayleigh-Jeans approximation expressed in terms of the brightness temperature T_c for the continuum source. At the Earth at a distance D, the observed flux in excess of that due to the continuum source can then be expressed as

$$S(v) = (2v^2kT_c/c^2D^2)\int db\, dz\{\exp\left[\tau(v, b, z)\right] - 1\}$$
$$\equiv (2v^2kT_c/c^2D^2)HR_o\mathscr{A} \quad (9)$$

where $\mathscr{A}$ is the "amplification factor" that we calculate and R_o is the mean radius of the masing ring. This factor $\mathscr{A}$ is approximately the amplification of the flux from the continuum source [that is, $S(v)/S^C$] and would have exactly this meaning if the dimensions of the continuum source were $H \times R_o$. For comparison to certain observational data (see

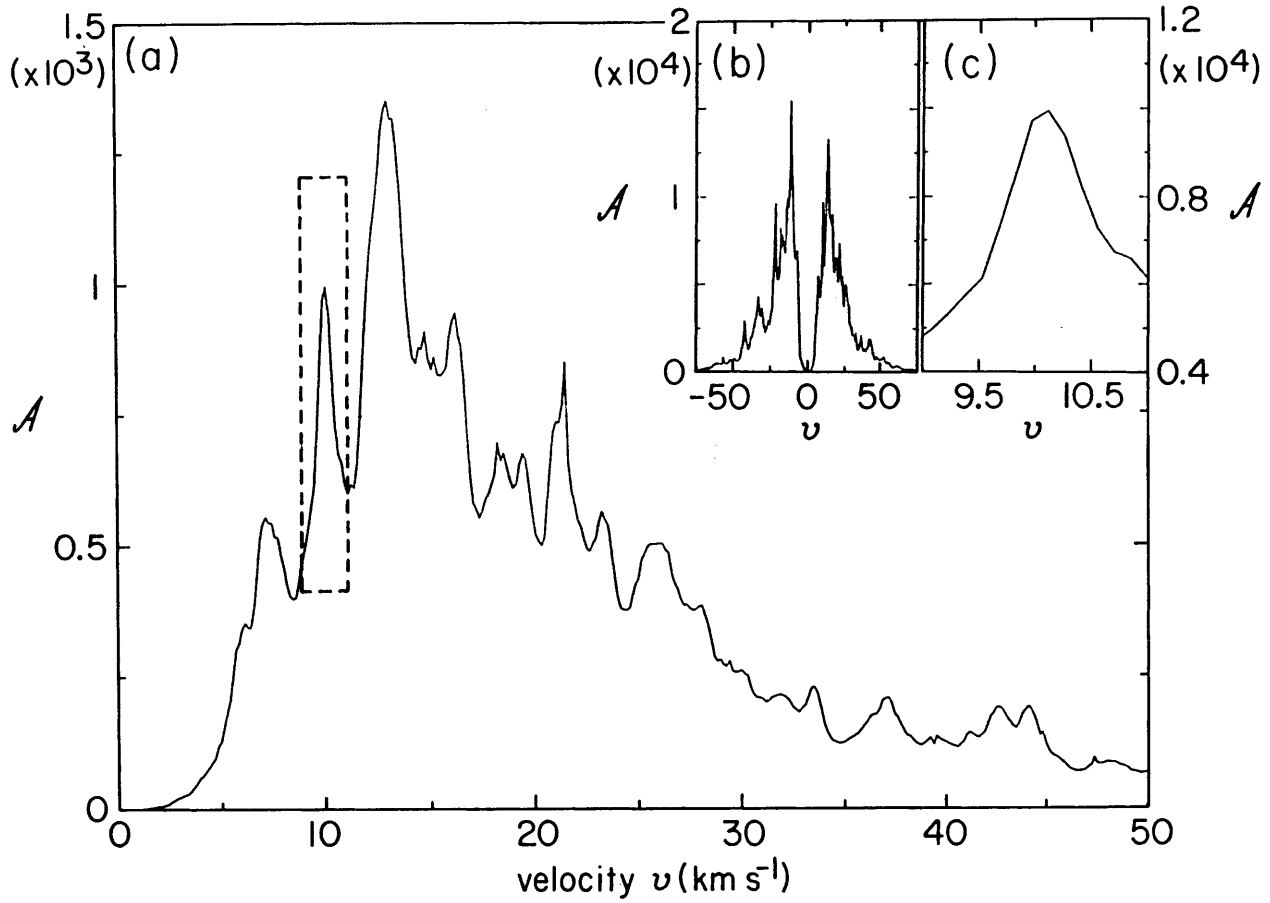


FIG. 2.—Representative spectrum from the calculations demonstrating the irregular, narrow microstructure and how absorption can create the minimum at the center of the spectrum. (*a*) The side of the full spectrum in panel (*b*) at positive velocities is expanded to show the microstructure. (*c*) The feature outlined by broken lines in panel (*a*) is further expanded to show the narrow ($\simeq 1$ km s^{-1}) full width of the feature. The spectrum is presented in terms of the amplification factor $\mathscr{A}$ that we compute and that is essentially the ratio of the observed brightness temperature to the brightness temperature T_c of the background continuum source vs. Doppler velocity v(km s^{-1}). For this spectrum $(\Delta R/R_o) = 0.2$ and $\sigma_t = 6$ km s^{-1}.

§ 3.4), we also consider the maser emission as a function of impact parameter

$$F(v, b) = \int dz[I(v, b, z) - I^C] . \tag{10}$$

In summary, within the foregoing formulation the calculations depend on the three parameters that represent (1) the dispersion σ_t in the turbulent velocities, (2) the opacity κ_o, and (3) the radial extent ΔR of the masing region. We will return to a discussion of limitations in the formulation itself. In certain computations, we wish to demonstrate the influence of absorption by H_2O molecules for which the 6_{16}–5_{23} transition is not inverted, but simply has a thermal ratio of the populations. To do this, a second ring is introduced at larger radii with an opacity coefficient κ_o that is negative. The parameters $v_{\rm th}$ and σ_t are likely to assume different values in this ring (and are different in the spectrum that is presented) from their values in the masing ring.

3. CALCULATIONS AND THEIR COMPARISON TO OBSERVATIONS

3.1. *General Considerations*

A representative spectrum of the maser flux from our calculations is presented in Figure 2 together with representative spectra from the observations of NGC 4258 in Figure 3. Numerous other spectra are available from observations

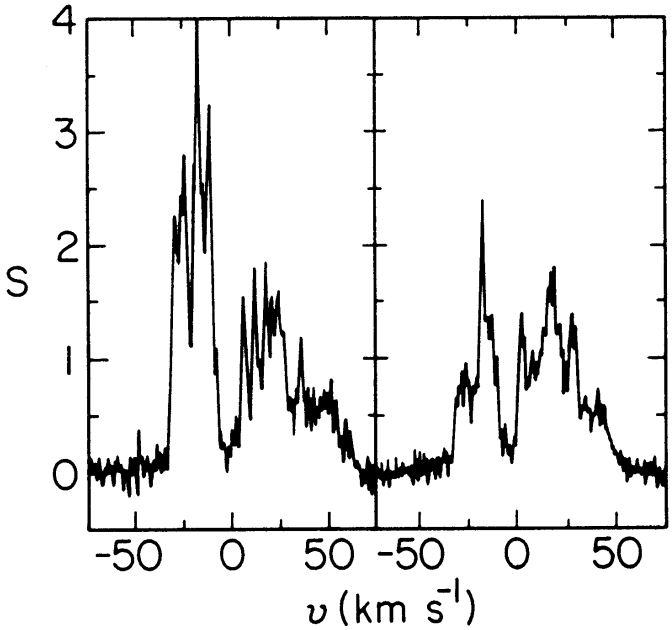


FIG. 3.—Representative observational spectra for the 22 GHz water masers near the systemic velocity in the circumnuclear accretion disk of NGC 4258 for comparison to our calculations. Note the minimum at the center and the difference between the spectra at different epochs (from R. Becker, C. Henkel, & T. L. Wilson 1995, private communication). Other examples can be found in references in the text to observational papers.

over the past decade or so (e.g., Moran et al. 1995; Nakai et al. 1995). The main characteristic to be noted at the outset is the ability of the calculations to create an irregular spectrum with microfeatures that are generally similar in appearance to the observed spectrum. In particular, despite being calculated with a turbulent velocity σ_t of 6 km s^{-1}, the line breadths of the microfeatures can be as narrow as the 1–2 km s^{-1} (FWHM) reported for the observed spectra. This can be understood. The bulk of the power (which mainly determines σ_t) in the Kolmogorov distribution is at long wavelengths. In contrast, the exponential sensitivity of maser amplification to optical depth leads to much smaller sizes for masing features. Hyperfine structure of the 22 GHz transition is ignored in the calculations here and would be expected to increase the widths of the microfeatures by a few tenths of a kilometer per second (Nedoluha & Watson 1991). Calculations in Figure 9 demonstrate that similarly narrow microfeatures occur for σ_t up to at least 10 km s^{-1}. Further, the calculated range of Doppler velocities from which significant flux is evident in the full spectrum is similar to that of the observed spectrum ($\simeq$80 km s^{-1}). As we discuss below, the magnitude of the flux also is compatible with the observed flux.

The observed spectra of NGC 4258 exhibit a persistent, narrow dip at the systemic velocity that resembles an absorption feature. Its strength varies—it can be essentially unnoticeable or it can divide the spectrum into two distinct features as shown in Figure 2. Unless absorption is included, this feature is not consistently reproduced in any spectra that we have calculated. To demonstrate how the calculations can reproduce this characteristic of the observed spectra as well, absorption in a second ring at larger disk radii has been incorporated to obtain the spectrum in Figure 2. At the center (impact parameter $b = 0$), the projection of the Keplerian velocity along the line of sight $v^{\rm K}$ is the same for the absorbing and masing rings. With increasing distance along the plane from the center (increasing $|b|$), the $v^{\rm K}$'s in these two rings become increasingly different due to the shear of the Keplerian velocities. Hence the absorption has its greatest effect at the center in reducing the maser flux. A dip or minimum in the spectrum is thus created (Watson & Wallin 1994). Since a consideration of absorption introduces additional uncertain parameters, except for demonstrating its possible effect in Figure 2, we ignore it in computing the spectra that are presented in the remainder of this investigation. We reason that basic characteristics of the observed spectra can be beneficially examined without a quantitative understanding of this dip at the center of the spectrum. In practice, we expect that some turbulence is likely to be present in the absorbing gas as well, which (along with the turbulence in the masing gas) will create variations in the appearance of this minimum from time to time.

At a superficial level of comparison, calculations that seem to agree with the observations of NGC 4258 can be made for a wide range of the values for the uncertain parameters σ_t, κ_o, and ΔR. To attempt to utilize the observational data to restrict further the values of these quantities, and thus to delineate the nature of the masing disk, we will focus in some detail on the following aspects of the calculated and observed maser spectra: (1) restrictions on the amplification implied by the peak in the observed flux combined with the range of likely brightness temperatures of the continuum radiation that is being amplified; (2) the range of Doppler velocities from which emission is observed in the full spectrum; (3) the relative importance of sharp "spikes" in the appearance of the spectrum; and (4) the scatter in the plot of Doppler velocities versus impact parameter. From the observed brightness of the maser flux, justification is provided for the premise that unsaturated masing can be an adequate approximation. Reasoning is also presented that turbulence on spatial scales smaller than resolved by our 512 × 512 × 32 grid is likely to disappear. First, however, we discuss what can already be said from other considerations about the relevant quantities.

The radial extent ΔR for the masing gas.—The observational data for v versus b for the masers near the systemic velocity of NGC 4258 fall along a straight line with only a small scatter. The slope of this line is a measure of the mean radius R_o at which the gas is located and the scatter provides a measure of the radial extent of the masing gas. By assuming that the entire scatter is due to variations in radius r in equation (7), estimates for ΔR have been made and range from about 30% to a few percent of R_o (Greenhill et al. 1995; Moran et al. 1995). We note that the latter estimate seems to be based on only a limited portion of the disk where the scatter is particularly small (see Fig. 4 of Moran et al. 1995). These assessments of ΔR also are based on data at only a few epochs and the spectrum is known to vary significantly. For masing by a uniform Keplerian disk (constant κ_o and no turbulent velocities) the radius that is obtained from the slope of b versus v will be at essentially the outer radius (here, $R_o + \Delta R/2$) of the masing gas in the limit of unsaturated masing (Watson & Wallin 1994). In contrast, for fully saturated masing the inferred value for the radius would be near that of the inner radius (Watson & Wallin 1995). A goal of the investigation here is thus to assess how inferences from the data about R_o and ΔR might be altered when a quantitative description is utilized for the irregularities in the masing gas.

The thickness H for the masing gas is not resolved.—Observations determine the locations of the maxima in maser emission as a function of the distance perpendicular to the plane of the disk. These maxima are interpreted to lie within 10^{15} cm of the plane of the disk. The possibility exists, nevertheless, that H is greater, since the actual extent of the emission is only known to be less than the VLBI resolution (2×10^{16} cm). Determinations of H may also be susceptible to radiative transfer effects, analogous to the well-known result that the apparent sizes of spherical masers are smaller than their actual sizes (e.g., Emmering & Watson 1994 for recent work). Finally, these observations only measure the thickness of the masing gas. The disk may also contain additional gas above and below the masing layer.

The rms turbulent velocity σ_t.—Deviations of 3.5 km s^{-1} (rms) have been reported between the observed Doppler velocities of the high-velocity components of the NGC 4258 masing disk and the expected Keplerian velocities for these components if they are located at radii equal to the impact parameters at which they are observed (Moran et al. 1995). These deviations may be an indication of turbulent velocities that are comparable to or exceed the sound velocity. At 500 K, the isothermal speed of sound in a gas with molecular hydrogen and atomic helium in cosmic abundance proportions is 1.3 km s^{-1}. Radiative transfer and excitation effects might also be imagined which cause the observed rms scatter in Doppler velocities of the maser radiation to

be greater or smaller than the actual turbulent velocities in the gas. Supersonic turbulence can make a significant contribution to the pressure that in turn is reflected by the thickness H of the disk. In the thin-disk approximation that is believed to be well satisfied for NGC 4258, this leads to a limit (e.g., Frank, King, & Raine 1992, p. 74)

$$\sigma_t \lesssim (H/R_o)V^{\rm K} \tag{11}$$

in which $V^{\rm K}$ is the full Keplerian velocity of rotation ($\simeq 1000$ km s^{-1} for the systemic emission). As noted above, we interpret the observational data as failing to exclude (H/R_o) at least as large as about 0.01 and hence σ_t up to 10 km s^{-1}. Inferences about the magnitude of σ_t with its implication for the viscosity in accretion disks is a focus of our investigation.

The amplifying maser opacity κ_o.—The simplification that κ_o is a constant may seem to be the most extreme idealization of our calculation. Masing features in our own Galaxy can be spatially resolved down to quite small scales ($\simeq 10^{13}$ cm), which has tended to lead investigators to think in terms of similarly small scales for the spatial variation of the pumping. Since the earliest investigations, this pumping has often been associated with enhanced temperature and densities due to a strong shock wave of some type (e.g., Schmeld, Strelnitskij, & Muzylev 1976). We (Collison & Watson 1995; Desch et al. 1998) and others (Neufeld, Maloney, & Conger 1994) have reasoned that the physical conditions necessary for water masers in circumnuclear environments (and especially in NGC 4258) are likely to be a result of X-ray and perhaps viscous heating. Unlike strong shock waves, these mechanisms can create the physical conditions for water masers that vary only slowly on spatial scales comparable to the ΔR that we utilize (2–8 $\times 10^{16}$ cm). Representative calculations yield a net pump rate for creating inverted populations of approximately 1 cm^{-3} s^{-1}, which leads to a population difference of about 10 cm^{-3} between the upper and lower masing states (Wallin & Watson 1997). At a kinetic temperature of 500 K, $\kappa_o \simeq 1.5 \times 10^{-14}$ cm^{-1}, which yields $\tau(0,\ 0,\ 0) = \kappa_o \Delta R = 600$ ($\Delta R = 4 \times 10^{16}$ cm) for the optical depth at $v = 0$ and $b = 0$ when there is no turbulence. Uncertainties in the gas density, chemical composition, temperature, etc. easily cause order of magnitude uncertainty in κ_o. This calculated pump rate is in general agreement with the observed luminosity of NGC 4258 (Wallin & Watson 1997), but again, there is uncertainty in the comparison due to poor knowledge about the angle into which the maser radiation is beamed and about the volume of the masing gas. In practice, we determine the allowable range for κ_o (through the amplification factor $\mathscr{A}$) from the requirement that the calculated and observed values for the peak maser flux be in agreement. The values for κ_o inferred in this way are consistent with the κ_o's cited above, which are obtained from a detailed evaluation of the pumping.

The amplification factor $\mathscr{A}$.—Utilizing the observed S(0) $\simeq 2$ Jy in equation (9) yields

$$(H/4 \times 10^{15}\ {\rm cm})T_c \mathscr{A} = 10^{11}\ {\rm K}\ . \tag{12}$$

A strong, unresolved (on a scale of 10^{17} cm) continuum source ($T_c \gtrsim 10^7$ K is detected near the nucleus of NGC 4258 but is offset from the location of the masers (Herrnstein et al. 1997). A symmetrically located source would lie behind the masers and would be expected from certain ideas about jets. It is not detected and thus must be weaker by a factor of about 10 or more, perhaps due to absorption between this source and the masing gas. Maser emission extends about 4×10^{16} cm along the plane of the disk. The putative continuum source being amplified is presumably at least this large. Hence, the upper limit for T_c in equation (12) is then also about 10^7 K. At the other extreme, it seems that the brightness temperature of the continuum emission from the neighborhood of a (mildly) active galactic nucleus should be at least the kinetic temperature of H II regions (10^4 K). We thus limit our attention to parameters for which $10^4 \lesssim \mathscr{A} \lesssim 10^7$, which is determined mainly by the effective mean optical depth $\kappa_o \Delta R/(1 + 2\sigma_t^2/v_{\rm th}^2)^{1/2}$ at the center of the spectrum and the center of the disk ($v = 0$, $b = 0$).

The degree of maser saturation.—Saturation occurs when stimulated emission due to the maser radiation is competitive with all other processes that deplete the populations of the masing states. The rate for the relaxation of molecular velocities is at least this rapid (Goldreich & Kwan 1974; Anderson & Watson 1993). For the 22 GHz transition, the representative rate for stimulated emission is

$$R_s = (c^2 A/8\pi h\nu^3) \int I\, d\Omega = (AkT_c/4\pi h\nu) \int \exp\,(\tau) d\Omega\ , \tag{13}$$

where the integration of the maser intensity I at line center is over the solid angle viewed by a molecule at the side of the masing region from which the observed radiation emerges. The angular integration within the plane can be replaced by the integration over impact parameters as in equation (9) so that

$$R_s \simeq (AkT_c/4\pi h\nu)\mathscr{A}\Delta\phi = (c^2 D^2 AS(0)/8\pi h\nu^3 HR_o)\Delta\phi\ , \tag{14}$$

where $\Delta\phi$ is the angular spread of the beam measured perpendicularly to the disk. This is uncertain, but would be expected to be determined by the thickness of the disk so that $\Delta\phi \simeq H/\Delta R$. Inserting the numerical values yields $R_s \simeq 1$ s^{-1} (note that this R_s is not dependent upon the size of the unresolved emission region for $v = 0$ maser radiation.) The decay rate Γ for the masing states due to all other processes is commonly also taken to be 1 s^{-1}. Calculations for the effect of saturation on the rebroadening of the spectral lines of maser radiation demonstrate that saturation has only a modest effect when R_s is less than or equal to the rate for velocity relaxation (see Fig. 1 of Nedoluha & Watson 1991 and note that $R_s = 1$ s^{-1} corresponds to $T_b \Delta\Omega = 10^{10}$ K sr in that figure). Thus while saturation is likely not to be completely negligible according to the foregoing assessment, there is reason to believe that its effect can be marginal for the spectral properties. An analogous calculation including fully the effects of saturation would be incomparably more difficult.

Grid size.—The 512 grid points in the plane of the disk that we utilize in most computations span a distance of 8×10^{16} cm in the disk. Length scales down to approximately 10^{14} cm are thus delineated. It is likely that spatial variations in the velocity field are intimately connected with irregularities or waves in the magnetic field in the molecular gas in diffuse astrophysical environments. Compelling evidence exists that this is the case for gas clouds relevant in star formation. A minimum wavelength for such disturbances commonly is based on dissipation by ambipolar diffusion,

$$\lambda_c \simeq \pi V_{\rm A}\, t_{\rm ni}\ , \tag{15}$$

which is obtained from the requirement that the highest frequency $\omega_c \simeq \boldsymbol{k} \cdot \boldsymbol{V}_A$ be limited by the ion-neutral collision time $t_{ni} \simeq 10^7$ s/(n_i/100 cm^{-3}) for the density of ions n_i (e.g., Spitzer 1978, p. 295). Here, k is the wavenumber and V_A is the Alfvén velocity. The relevant limitations readily allow V_A up to 10 km s^{-1} (see § 4)—the maximum σ_t in our calculations. The inverted populations necessary for masing are expected to disappear when the collisional excitation by charged particles dominates over that by neutrals, which occurs when the fractional ionization exceeds about 10^{-5}. Various independent considerations suggest that the total gas density may be about 10^8 cm^{-3} (Desch et al. 1998; Wallin & Watson 1997). Then $\lambda_c \simeq 10^{14}$ cm occurs for a fractional ionization that is 1/30 of the maximum allowable value. An estimate can be made for the density of ions n_i that results when the energy to heat the masing gas to the necessary 400 K or so is provided by X-rays—a possibility that has been discussed. With cooling rates from Desch et al. (1998), our estimate for n_i is compatible with that ($\simeq$30 cm^{-3}), for which $\lambda_c \simeq 10^{14}$ cm in equation (15).

Limited computations have been performed with larger grids (up to 2048 in one dimension). The appearance of these spectra is similar to the appearance of those presented here. Such computations require considerably more computer time and larger computer memories.

3.2. *Doppler Breadth of the Full Spectrum*

A basic restriction on the calculations is that the range of Doppler velocities within which maser emission occurs should agree with the observations. We adopt 80 km s^{-1} as typical of the observational data (see Fig. 2). Note that this is not a half-breadth. Because of the irregularity and variation in both the observed and calculated spectra, it does not seem that a half-breadth is useful. By examining the calculated irregular spectra for representative choices of the relevant parameters, we find that what we somewhat subjectively judge as the range of emission (corresponding in appearance to the observed "range") is approximately the width of the average of a large number of the realizations of the spectrum at about one-fifth of the peak of this average spectrum. This width is then calculated and presented in Figure 4 as a basis for comparison to the observations. The widths obtained in this way are in excellent agreement with those calculated by ignoring turbulence altogether but with v_{th} increased to $(v_{th}^2 + 2\sigma_t^2)^{1/2}$—a common way to incorporate the effects of turbulence into the transport of spectral line radiation. For simplicity, some of the calculations for Figure 4 are performed in this approximation because a large number of realizations are necessary to obtain an averaged spectrum that is smooth.

To obtain the observed range of emission without supersonic turbulence, the radial extent must be quite small $\Delta R \lesssim 0.05 R_o$. Conversely, for ΔR to be as large as $0.2R_o$, σ_t must be greater than about 6 km s^{-1} (vs. 1.3 km s^{-1} for the isothermal sound velocity at 500 K). Calculations are presented (Fig. 4) for two choices of the amplification $\mathscr{A}$ that tend to encompass the likely amplifications. Maser flux decreases as a function of distance along the disk from the center because the difference increases between the Keplerian velocities at the inner and outer edges of the masing ring. With increasing turbulence, this difference is relatively less important and the maser flux decreases less rapidly leading to larger widths with larger σ_t in Figure 4. When ΔR is smaller, the difference in the Keplerian velocities through the ring is also smaller and has a lesser effect on the spectrum. Hence, the width increases as ΔR decreases (when ΔR goes to zero, the flux does not decrease at all with increasing impact parameter until the edge of the continuum source is reached).

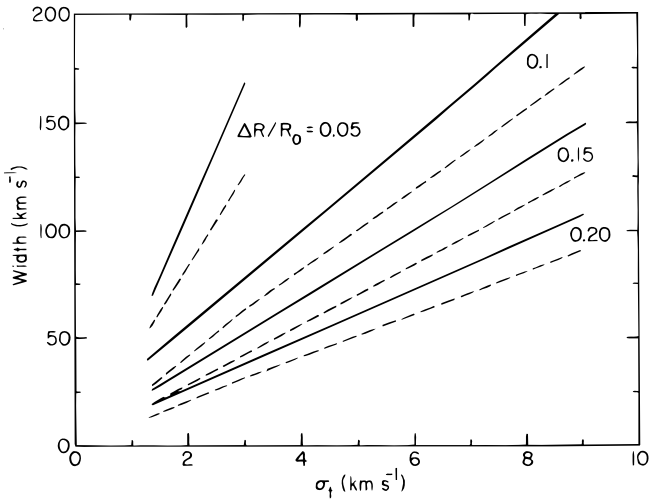


FIG. 4.—Range of Doppler velocities at which calculated maser emission occurs as a function of the turbulent velocity parameter σ_t for several values of the radial extent ΔR of the masing region. The analogous range from the observational data is approximately 80 km s^{-1}. The solid and broken lines, respectively, represent calculations for amplification $\mathscr{A} = 10^6$ and 10^3.

In presenting the widths in Figure 4, T_c is treated as constant. The extent of the maser emission along the plane of the disk might be determined by (and thus would be the same as) the size of the background continuum source. Under these circumstances, the widths presented in Figure 4 should be viewed as upper limits. That is, only the σ_t and ΔR are considered to be excluded when the calculated width is less than about the 80 km s^{-1} that we adopt as representative of the observational data. Although σ_t and ΔR are not determined uniquely, the possibilities are restricted.

3.3. *Appearance of the Spectrum*

In Figures 5–9, we present a number of calculated maser spectra for various choices of the relevant quantities σ_t, ΔR, and $\mathscr{A}$ (which replaces κ_o as a more useful way to describe the dependence on pumping). In these choices we are guided by the general constraints from § 3.1, by the constraints relating σ_t and ΔR to obtain a width for the full spectrum that agrees with observation as discussed in § 3.2, and to some degree by constraints that will be presented in § 3.4. Various statistical realizations are given for each set of choices for the parameters. The random numbers used to create the *a* (or *b*, or *c*, or *d*) realization are the same in all of these figures. Calculations utilizing the modified turbulent power spectrum (the anisotropic spectrum of eq. [5]) are presented in Figures 8 and 9.

We propose to characterize the maser spectra qualitatively according to the relative importance of the sharp spikes in comparison to the underlying merged emission (i.e., the emission in the minima between the spikes). The latter is sometimes designated as a "pedestal" in the literature.

There do seem to be some meaningful trends in the appearance of the spectra as a function of the relevant

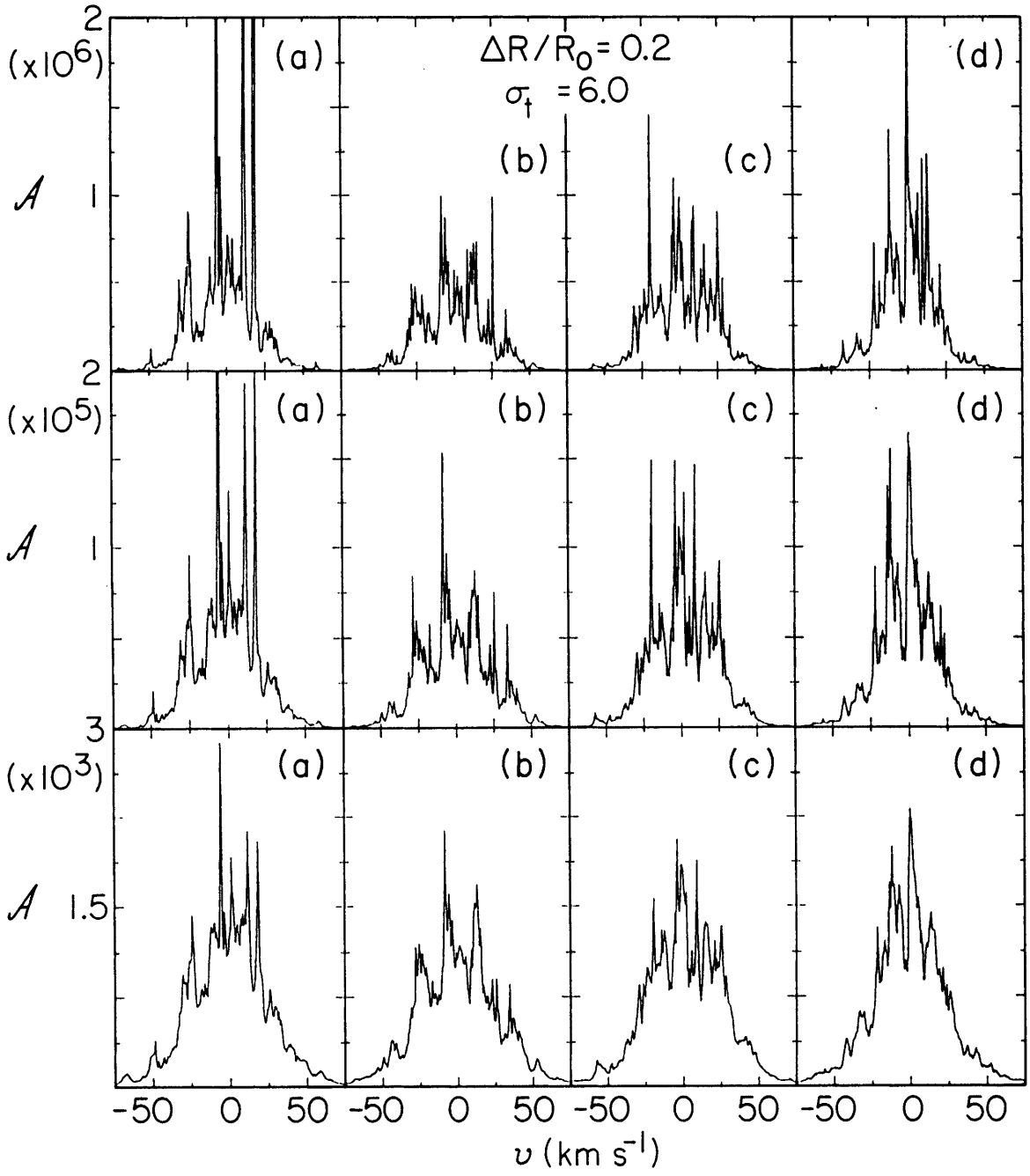


FIG. 5.—Representative maser spectra computed for four successive realizations (*rows*) of the statistical velocity field at three values (*columns*) for the opacity parameter κ_o. Flux expressed in terms of the amplification $\mathscr{A}$ vs. Doppler velocity v (km s^{-1}) is presented. Here $\Delta R = 0.2R_o$, $\sigma_t = 6$ km s^{-1}, and the "isotropic" distribution is utilized for the turbulent velocities. The labels *a*, *b*, *c*, and *d* designate the ensemble of random numbers used to create the particular statistical realization. These ensembles are the same in Figs. 5–9.

parameters. With decreasing σ_t, the relative importance of spikes to the pedestal emission tends to increase. There is also some tendency for the relative importance of the spikes to increase with increasing amplification $\mathscr{A}$. It appears that there are fewer sharp spikes in those computed with the modified, anisotropic spectrum for the velocities (eq. [5]), which may better reflect the importance of the rotation. Unfortunately, the appearance of the observed spectrum of NGC 4258 changes sufficiently from epoch to epoch (e.g., R. Becker, C. Henkel, & T. L. Wilson 1995, private communication; Nakai et al. 1995) that it is difficult to conclude with complete confidence that any of the values from the range of values examined for the key parameters (σ_t, ΔR, and $\mathscr{A}$) are clearly excluded. That is especially true when the possible effects of absorption indicated in Figure 2 are considered. As noted previously, absorption is not included in the computation of the other spectra. From the discussion of § 3.2, ΔR must be small if the turbulence is to be subsonic. Such spectra are shown in Figures 7 and 8. The relative importance of sharp spikes does seem to be greater in these than in the observed spectra, especially for the "standard" velocity spectrum of equation (10) that is utilized for the spectra in Figure 7. The spectra computed for larger σ_t and ΔR (Figs. 5, 6, and 9) seem to appear more similar to the observations (allowing for the absorption minimum). Sharp spikes are less prominent in those computed with the modi-

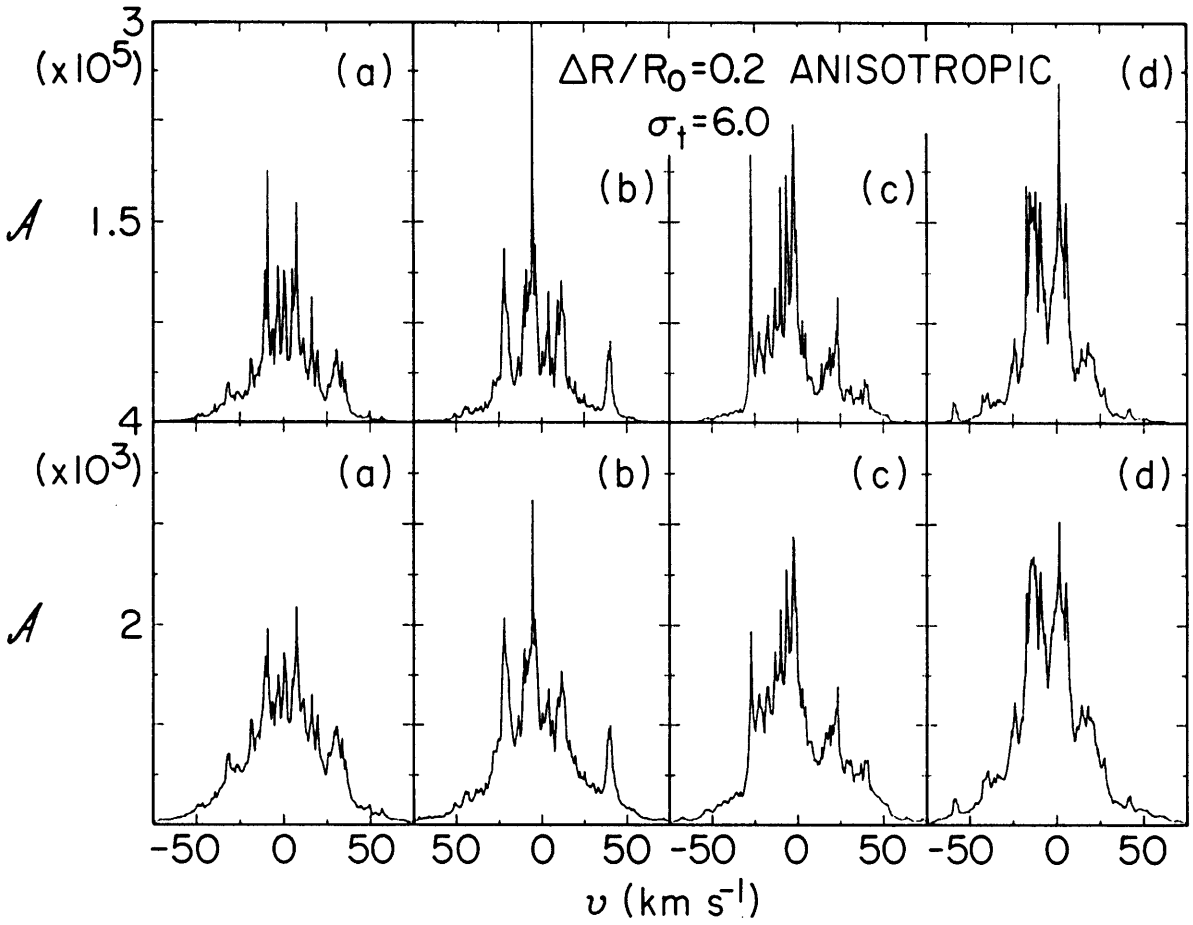


FIG. 6.—Same as Fig. 5 but that the "anisotropic" distribution for turbulent velocities is utilized and computations are made for only two choices of the opacity parameter κ_o ($\Delta R = 0.2R_o$ and $\sigma_t = 6$ km s^{-1}).

fied (eq. [5]) description of the velocities, and seem to resemble better the observed spectra. We conclude that the appearance of the spectra is weak evidence that the turbulence must be supersonic. As noted previously, the plausible range for T_c for the background continuum source is about 10^4–10^7 K implying $\mathscr{A} \simeq 10^4$–10^7. Again, there is a weak tendency for lower $\mathscr{A}$ to be preferred based on a comparison to typical observations because the spikes are somewhat less prominent in these spectra. In contrast, the tendency for quite intense spikes to be produced in some realizations with larger average amplifications $\mathscr{A}$ is reminiscent of flares that have been reported (see Fig. 5).

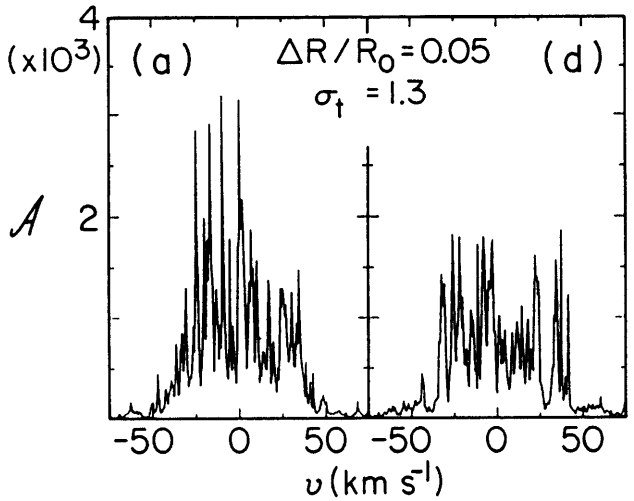


FIG. 7.—Same as Fig. 5 but that $\Delta R = 0.05R_o$, $\sigma_t = 1.3$ km s^{-1} is close to the isothermal sound velocity and the turbulent velocities are "isotropic" (only two statistical realizations are shown).

A description of the maser spectra in terms of quantitative, statistical parameters is desirable for a comparison to the observations. A limited effort has been made, although a useful statistical description has not been identified.

3.4. *Impact Parameter versus Doppler Velocity*

To compare further to observational data that are available, we find the impact parameter $b_m(v)$ at which the maximum emission occurs for each Doppler velocity. That is, $b_m(v)$ is found from the requirement that

$$\left.\frac{\partial F(v, b)}{\partial b}\right|_{b=b_m} = 0 , \tag{16}$$

where $F(v, b)$ is defined in equation (10). The analogous observational data are available in Greenhill et al. (1995, Fig. 7), Miyoshi et al. (1995, Fig. 3), and Moran et al. (1995, Fig. 3). If all of the masing were occurring at a single radius and there were no turbulence, the data in Figure 10 would lie exactly on a straight line. The scatter is thus a measure of the finite extent of ΔR and of the irregularities in the medium. From equation (7), the slope of the $b_m(v)$ curve determines an "average" value for the radius R_o at which the maser radiation is created. Without turbulence, the slope of the analogous $b_m(v)$ versus v curve would instead

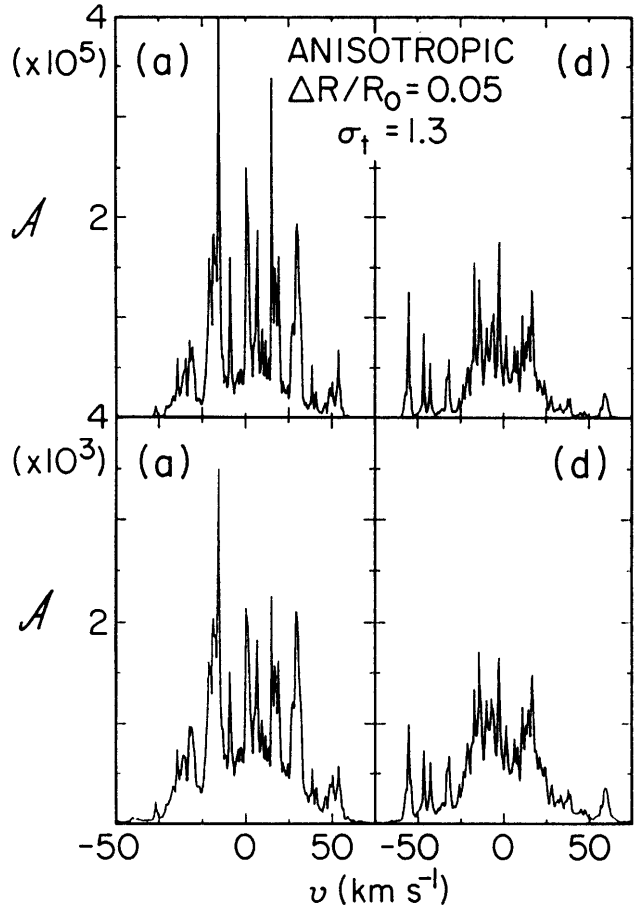


FIG. 8.—Same as Fig. 7 but that the turbulent velocities are "anisotropic," and spectra are shown for two choices of the maser opacity parameter $\kappa_o(\Delta R = 0.05R_o$ and $\sigma_t = 1.3$ km s^{-1}).

yield essentially the outer radius for unsaturated masing (Watson & Wallin 1994) and essentially the inner radius for fully saturated masing (Watson & Wallin 1995). In our calculations for unsaturated masers with turbulent velocities, the best-fit slope also corresponds essentially to the outer

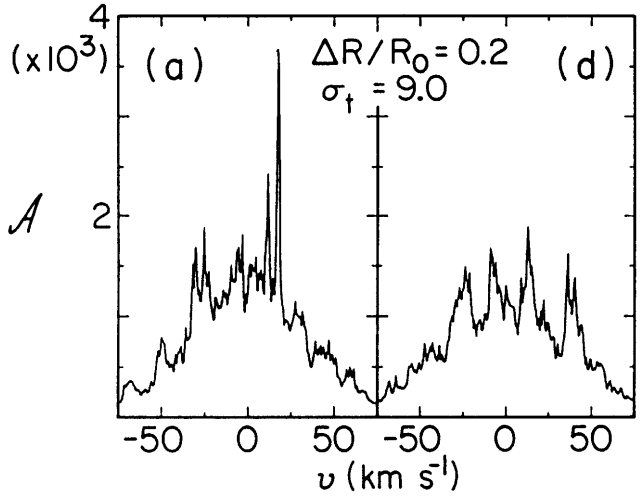


FIG. 9.—Same as previous figures but that here $\Delta R = 0.20R_o$ and $\sigma_t = 9$ km s^{-1}. "Isotropic" turbulent velocities are adopted, and only two statistical realizations are shown for a single choice of the opacity parameter κ_o.

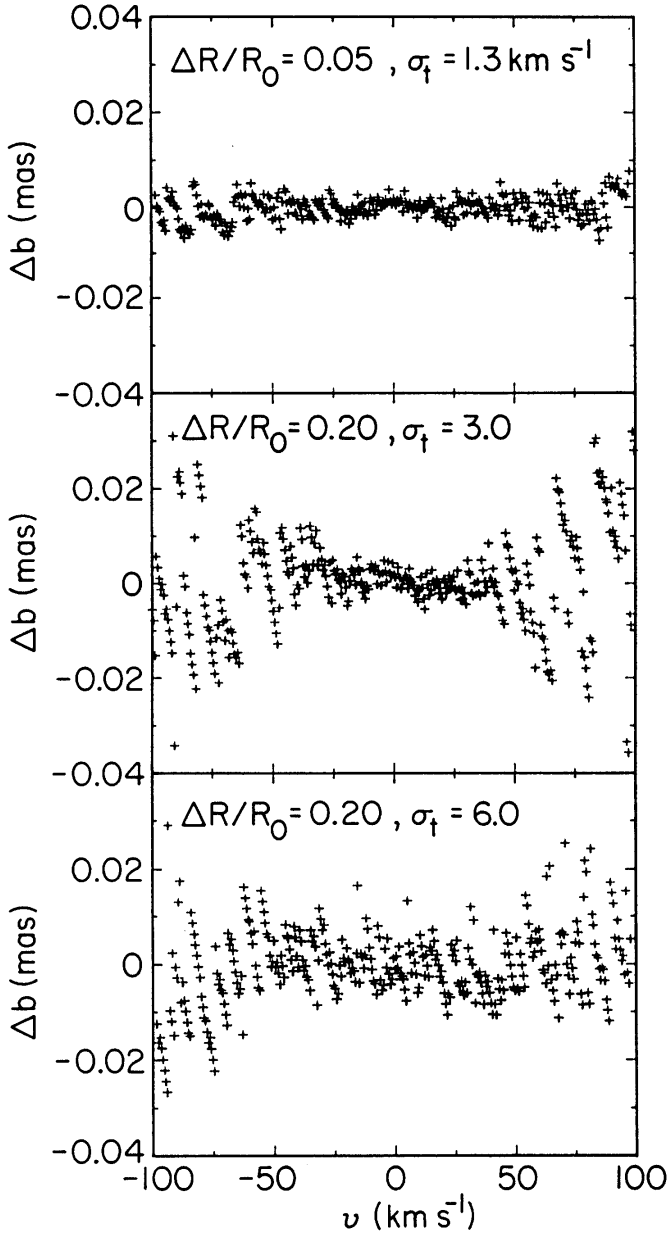


FIG. 10.—Deviations from the Keplerian relationship. The deviation $\Delta b_m(v)$ from the best-fit straight line for computed values of $b_m(v)$ for a representative statistical realization, but for different ΔR and σ_t. For comparison to observations, the Δb_m are assumed to be at the distance of NGC 4258 and are expressed in milliarcseconds. Here, the deviations for a narrow masing ring with low turbulence are contrasted with those for wider rings with higher turbulence.

radius of the masing ring. To display the scatter best, what is plotted in Figure 10 is the difference between the individual b_m and the straight line that best fits all of the b_m in each realization.

As with the observational data, there is a tendency for the points in Figure 10 to scatter away from a straight line and for this scatter to increase in either direction away from the center ($b = 0$) of the disk for certain choices of σ_t and ΔR. We infer a characteristic maximum deviation from an examination of observational data (Moran et al. 1995, Fig. 3; Greenhill et al. 1995, Fig. 7) of ± 0.03 mas toward the sides of the spectrum. Near the center of the spectrum, the deviation in the observational data tends to be smaller by a factor of 2 or more. The lack of significant scatter in the top

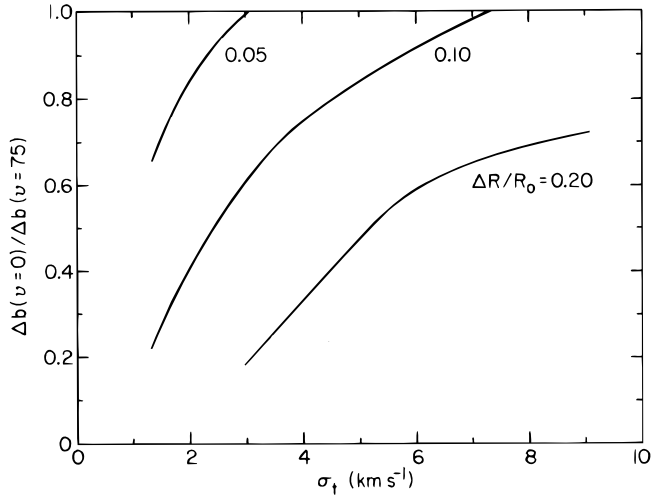


FIG. 11.—Ratio of the value at the center ($v = 0$) to that at the side ($v = 75$ km s^{-1}) is shown for the rms of the deviations Δb_m obtained for a large number of statistical realizations, as a function of σ_t for masing rings with ΔR as indicated. There is negligible difference between these curves for the isotropic and the anisotropic velocity distributions that we utilize, or for the range of amplifications $\mathscr{A}$ that we consider.

panel in Figure 10 is thus compelling evidence against the lower (subsonic) turbulent velocities σ_t. Calculations are presented only for $\Delta R = 0.05R_o$ at $\sigma_t = 1.3$ km s^{-1} because only the smaller ΔR lead to sufficient width for the overall spectrum for the systemic emission at this value for σ_t, as discussed in § 3.2 (see also Fig. 4). In contrast, the analogous calculations with larger σ_t are in reasonable agreement with the limited observational data that are available concerning the scatter in b_m. Although we show only a single realization (at different σ_t and ΔR) in Figure 10, the behavior displayed in Figure 10 is representative of numerous other computations. As illustrated in Figures 10 and 11, these calculations indicate that the scatter in b_m increases as ΔR and σ_t increase, and that the ratio of scatter at the center to that at the sides decreases with increasing ΔR but increases with increasing σ_t. These variations can readily be understood. With increasing ΔR, the range in v^K encountered by a ray at fixed impact parameter increases. This increases both the scatter at the sides of the spectrum, as well as the ratio of this scatter to that at the center, since the range in v^K remains zero at $b = 0$ (and can be smaller than σ_t for b near zero) regardless of ΔR. Increasing the turbulent contribution σ_t tends to increase the scatter at all ΔR as expected for an additional contribution to the velocity dispersion. Since v^K depends on ΔR but σ_t does not, the calculated scatter approaches a value that is independent of ΔR as σ_t increases. While we focus on $\mathscr{A} \simeq 10^4$ in these figures as our best estimate from other information, as discussed earlier, we have verified that they are not altered significantly for other $\mathscr{A}$ within the likely range. This is not surprising in view of the relative insensitivity of the appearance of the spectrum to changes in $\mathscr{A}$ noted in § 3.3.

4. DISCUSSION

The strongest conclusions from the foregoing comparisons between the calculated and observed spectra for NGC 4258 are (1) plausible turbulent velocities can lead to irregular maser spectra that are similar in appearance to the observed spectra, including the quite narrow Doppler breadths down to 1–2 km s^{-1} even in the presence of rms turbulent velocities that are much greater; (2) from the Doppler breadth of the overall spectrum, the turbulence must be supersonic (relative to the sound speed in the masing gas) unless the radial extent of the masing ring is quite small (less than about 5% of the radius of the disk); (3) the scatter in the location and in the Doppler velocities of the emission features from that given by the Keplerian relationship (b_m vs. v) tends to exclude a small radial extent for the masing ring and thus indicates that the turbulent velocities are somewhat supersonic; (4) the rate for stimulated maser emission on the near side of the masing region is approximately 1 s^{-1}—the rate at which "saturated rebroadening" of the spectral lines begins to appear but is not yet a major effect; (5) the appearance and other characteristics of the calculated spectra are relatively insensitive to the amplification provided by the masing within the likely range of amplification factors. The spectra are consistent with the presence of a bright (10^7–10^8 K) continuum source that is being amplified, but also with a much weaker source. Absorption by thermalized water molecules in the disk outside of the masing ring can create a minimum at the center of the spectrum that is similar to what is observed.

Calculations here are based on the "simplest" premises about the turbulence and excitation of the maser as discussed in § 1 and elsewhere. The above conclusions have nevertheless been shown to be insensitive to certain plausible modifications to the turbulent velocity field (disk thickness, exact effects of anisotropy suggested by MHD simulations). Clearly, the possibility cannot be excluded that reasons will arise to support modifications in the velocity field and in the excitation that we have not considered. Such changes might well alter aspects of our interpretation, notably the need for supersonic turbulent velocities. Establishing at a quantitative level that our conclusions would be unchanged if the minimum scale length (λ_c in § 3.1) is smaller than is resolved by our grid size would place severe (and perhaps impossible) demands on available computer resources. In our limited computations with larger grids, the basic features of the resulting spectra are similar to those presented here.

A significant aspect of the interpretation of the disk in NGC 4258 based on our calculations is the implication that supersonic velocities are present in the masing medium. Supersonic turbulence suggests high viscosity and hence a substantial dissipation of heat in the masing gas (e.g., Shakura & Sunyaev 1973). It may be that this high viscous dissipation is, in fact, necessary to provide the heat to create the physical conditions for the masing. The energy available per unit surface area from this source is sufficient in magnitude based on the mass accretion rate implied by the luminosity of the presumed black hole at the nucleus of NGC 4258 (Desch et al. 1998). Efficient viscous dissipation also is necessary if accretion through the disk is to provide the infalling mass required in advective models of the inner disk of NGC 4258 (Lasota et al. 1996). We note again that the high-velocity features exhibit a deviation of 3.5 km s^{-1} rms from the Keplerian relationship (Moran et al. 1995), which may also be indicative of turbulent velocities that exceed the sound velocity ($\simeq 1.3$ km s^{-1}) in the masing gas. Although supersonic, the turbulent velocities can still be less than the Alfvén velocity, as is usually the relationship among these velocities in the dense molecular gas in star forming regions. The most reliable information about the strength of the magnetic field in the masing disk of NGC 4258 is an upper

limit of 300 mG based on a limit for the circular polarization in the high-velocity (side) maser features (Herrnstein et al. 1998) for which the Alfvén velocity is about 30 km s^{-1} at a representative gas density of $n_{H_2} = 10^8$ cm^{-3}. Sensitive upper limits to the linear polarization of this maser radiation are also available (Deguchi, Nakai, & Barvainis 1995; Herrnstein et al. 1998). However, inferences about the strength of the magnetic field based on the linear polarization are open to considerable doubt. The rate R_s for stimulated emission must be large enough that the degree of saturation is substantial in order that linear polarization can be a consequence of the presence of magnetic fields (see Fig. 7 of Nedoluha & Watson 1992; also Nedoluha & Watson 1990). Rebroadening of the spectral line must accompany a stimulated emission rate that is large enough that appreciable linear polarization will be created by the presence of magnetic fields. The 22 GHz masing transition of water has a minimum spectral line breadth of 1.5 km s^{-1} when fully rebroadened (Nedoluha & Watson 1991), whereas the line breadths of the high-velocity features can be smaller.

It is evident that further analysis along the lines of this paper, but for (1) the high-velocity components, (2) the time variations in the spectra, and possibly (3) the relationship between the magnetic field and the polarization of the maser radiation, is likely to yield additional information about the nature of the disk in NGC 4258 and of circumnuclear accretion disks in general.

We are grateful to a number of people who have aided this investigation in various ways. These include D. Balsara, G. Bryan, L. Greenhill, J. Herrnstein, K. Y. Lo, A. Mangalum, J. Moran, A. Pouquet, and R. Schult. Partial support was provided from NSF Grant AST 94-01348. B. K. W. is a NASA GRP Fellow.

REFERENCES

Anderson, N., & Watson, W. D. 1993, ApJ, 407,620
Brandenberg, A., Nordlund, A., Stein, R. F., & Torkelsson, U. 1995, ApJ, 446, 741
Collison, A. J., & Watson, W. D. 1995, ApJ, 452, L103
Deguchi, S., Nakai, N., & Barvainis, R. 1995, AJ, 109, 507
Desch, S. J., Wallin, B. K., & Watson, W. D. 1998, ApJ, in press
Dubinski, J., Narayan, R., & Phillips, T. G. 1995, ApJ, 448, 226 (DNP)
Emmering, R. T., & Watson, W. D. 1994, ApJ, 424, 991
Frank, J., King, A., & Raine, D. 1992, Accretion Power in Astrophysics (2d ed.; Cambridge: Cambridge Univ. Press)
Goldreich, P., & Kwan, J. Y. 1974, ApJ, 190, 27
Greenhill, L. J., Henkel, C., Becker, R., Wilson, T. L., & Wouterloot, J. G. A. 1995, A&A, 304, 21
Herrnstein, J. R., Greenhill, L. J., Moran, J. M., Blackman, E. G., & Diamond, P. J. 1998, in preparation
Herrnstein, J. R., Moran, J. M., Greenhill, L. J., Diamond, P. J., Miyoshi, M., Nakai, N., & Inoue, M. 1997, ApJ, 475, L17
Lasota, J.-P., Abramowicz, M. A., Chen, X., Krolik, J., Narayan, R., & Yi, L. 1996, ApJ, 462, 142
Lesieur, M. 1990, Turbulence in Fluids (2d. ed.; Dordrecht: Kluwer)
Miyoshi, M., Moran, J., Herrnstein, J., Greenhill, L., Nakai, N., Diamond, P., & Inoue, M. 1995, Nature, 373, 127
Moran, J., Greenhill, L., Herrnstein, J., Diamond, P., Miyoshi, M., Nakai, N., & Inoue, M. 1995, Proc. Natl. Acad. Sci., 92, 11427
Nakai, N., Inoue, M., Miyazawa, K., Miyoshi, M., & Hall, P. 1995, PASJ, 47, 771
Nedoluha, G. E., & Watson, W. D. 1990, ApJ, 354, 660
———. 1991, ApJ, 367, L63
———. 1992, ApJ, 384, 185
Neufeld, D. A., Maloney, P. R., & Conger, S. 1994, ApJ, 436, L127
Schmeld, I. K., Strelnitskij, V. A., & Muzylev, V. V. 1976, AZh, 53, 728
Shakura, N. I., & Sunyaev, R. A. 1973, A&A, 24, 337
Spitzer, L., Jr. 1978, Physical Processes in the Interstellar Medium (New York: Wiley)
Stone, J. M., Hawley, J. F., Gammie, C. F., & Balbus, S. A. 1996, ApJ, 463, 656
Wallin, B. K., & Watson, W. D. 1997, ApJ, 476, 685
Watson, W. D., & Wallin, B. K. 1994, ApJ, 432, L35
———. 1995, BAAS, 27, 1360